

## Helicity and Transport in Electron MHD Heat Pulses

R. L. Stenzel and J. M. Urrutia

Department of Physics, University of California, Los Angeles, California 90095-1547

(Received 20 October 1995)

Electrons are heated locally and temporally in a uniform magnetoplasma by applying a short current pulse to a loop antenna. The resultant heat pulse, satisfying electron MHD conditions ( $\omega_{ce}^{-1} \ll \Delta t \ll \omega_{ci}^{-1}$ ), generates helicity due to twisting of field lines by diamagnetic drifts. Heat convection and diffusion cool the pulse, which reduces its propagation to zero. The stationary temperature profile decays by cross-field transport conserving volume-integrated heat.

PACS numbers: 52.25.Fi, 52.30.-q, 52.50.Gj, 52.70.Ds

Heat transport and helicity generation in magnetized plasmas is a topic of general interest in laboratory and space plasmas. For example, it plays a role in the energy confinement of fusion plasmas [1] and the heating of the solar corona [2]. Here we are interested in an initial and boundary value problem where a plasma is heated locally and temporally in the regime of electron MHD. The temperature relaxation in space and time is controlled by conduction with anisotropic heat conductivities and convection by electron flows, i.e., currents. Experimentally, an electron heat pulse is injected and the resultant current system is measured with magnetic probes. The axially varying diamagnetic drift rotates the electron fluid across  $\mathbf{B}_0$ ; hence the fairly frozen-in magnetic field [3] is twisted and forms a finite-length flux rope observed to satisfy  $\nabla \times \mathbf{B} = k\mathbf{B}(\mathbf{r}, t)$ . Although the twist is small ( $\approx 20^\circ$ ) in the present experiment, it is possible to obtain large twists in hotter plasmas, e.g., in photospheric plasmas. A large twist could lead to reconnection and emission of low frequency whistlers transporting heat faster than Alfvén waves into the corona [4].

The experiment is performed in a large plasma column (1 m diam  $\times$  2.5 m) sketched in Fig. 1. It is a pulsed dc discharge (40 V, 500 A,  $t_{\text{pulse}} \approx 5$  ms,  $t_{\text{rep}} \approx 1$  s) produced with a 1 m diam oxide-coated cathode in argon (0.3 mTorr). In the quiescent, uniform, low-temperature, afterglow plasma ( $n_e \approx 2 \times 10^{11}$  cm $^{-3}$ ,  $kT_e \approx 0.5$  eV,  $B_0 \approx 15$  G, a short ( $\Delta t_{\text{FWHM}} \approx 0.2$   $\mu$ s) current pulse is applied to an insulated magnetic loop antenna (4 cm diam, two turns, axis  $\parallel \mathbf{B}_0$ ) or to a one-sided electrode. Time-varying magnetic fields associated with currents in the antenna and plasma are measured with a movable magnetic probe, recording ( $B_x, B_y, B_z$ ) simultaneously versus time at a given position. By repeating the highly reproducible discharge and moving the probe to different positions, the vector field  $\mathbf{B}(\mathbf{r}, t)$  is acquired and stored. The current density is calculated via Ampère's law,  $\mathbf{J} = \nabla \times \mathbf{B}/\mu_0$ , where the vacuum displacement current can be neglected. From the diamagnetic field, electron temperature changes as small as  $10^{-3}$  eV can be deduced. The background plasma parameters are measured with a Langmuir probe. Nonintrusive light-emission measurements quali-

tatively support the electron heating observed with *in situ* probes.

The electromagnetic field in the near zone of the antenna gives rise to strong electron heating, and excites a transient whistler wave pulse which propagates with  $v_{\parallel} \approx 1.5 \times 10^8$  cm/s along  $\mathbf{B}_0$  [5]. The front of the heat pulse advances along  $\mathbf{B}_0$ , slows down as the temperature decreases, and, finally, a stationary but decaying temperature profile is achieved. The present work focuses on the slow relaxation processes of the heated flux tube after the transient heating and wave processes have died out.

Figure 2(a) displays the time-varying magnetic field component  $B_z$  vs radial position,  $y$ , and time,  $t$ . At early times ( $t < 1.5$   $\mu$ s), the large amplitude signal is that of the applied pulse and the excited whistler wave transient. Subsequently, the long-lasting response is a diamagnetic field  $B_z$  caused by electron heating in the flux tube of the antenna. Because of the large dynamic range ( $4$  mG  $< B_z < 4$  G), the data have been taken at two different levels of sensitivity and connected at  $t = 5$   $\mu$ s. This avoids saturation of the peak values and the drowning of weak signals by digitization noise. The signals have also been digitally corrected to remove the droop introduced by the analog RC-integration employed in the preprocessing. The field distribution for  $y > 0$  and  $y < 0$  is almost identical, indicating reasonable azimuthal symmetry ( $\partial/\partial\theta \approx 0$ ), as

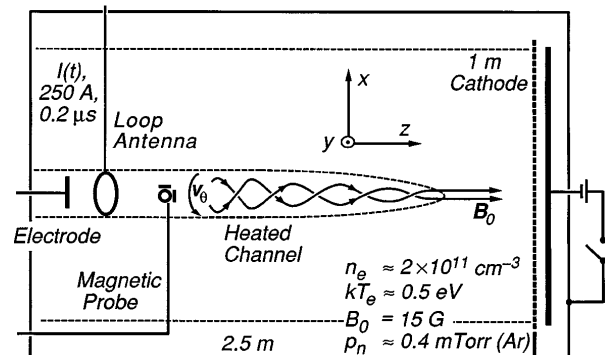


FIG. 1. Schematic of the experimental device, diagnostics, parameters, and field line twisting by diamagnetic drifts. Observed twists are smaller than displayed.

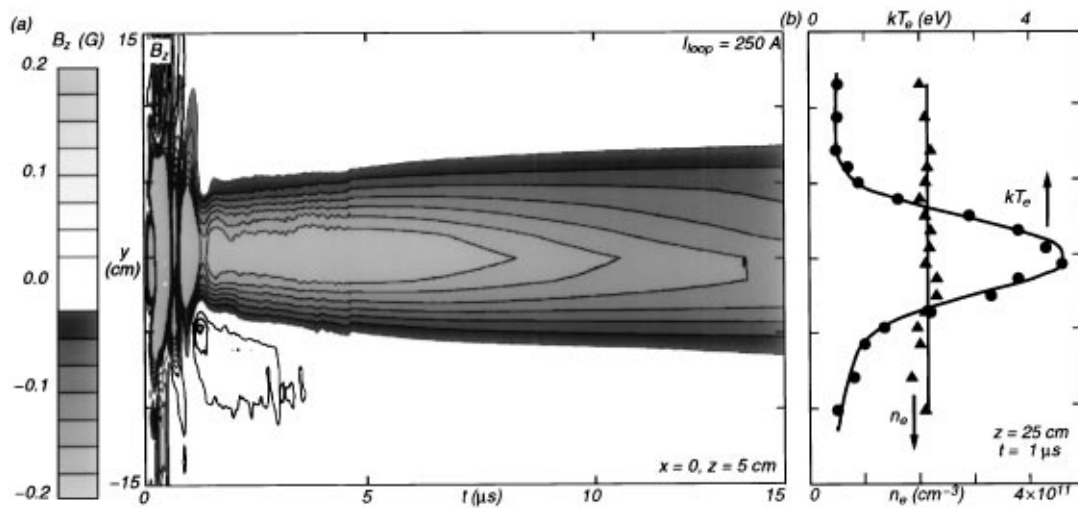


FIG. 2. (a) Perturbed magnetic field  $B_z$  vs position,  $y(\perp \mathbf{B}_0)$ , and time,  $t$ , showing the formation of a long-lasting diamagnetic signal as a result of electron heating by a short intense current pulse. (b) Probe-measured plasma parameters show electron temperature enhancement in the uniform plasma.

expected from the geometry of the antenna. In time, the width of the heated channel gradually expands, and the field strength slowly decreases due to radial and axial heat transport.

The plasma parameters are directly measured with probes. Figure 2(b) shows the radial density and temperature profiles at  $z = 5$  cm,  $t = 1 \mu s$ . No significant density changes are observed, but the electron temperature is strongly enhanced in the flux tube of the antenna. The former is expected since density enhancements due to ionization in a Maxwellian electron distribution with  $kT_e \approx 5$  eV occur at a rate  $\partial n_e / \partial t = n_0 n_e \langle \sigma_i v_e \rangle \approx 4 \times 10^{15} \text{ cm}^{-3} \text{ s}^{-1}$  where  $n_e \langle \sigma_i v_e \rangle \approx 4 \times 10^2 \text{ s}^{-1}$  is the ionization frequency in Ar [6], and  $n_0 \approx 10^{13} \text{ cm}^{-3}$  is the neutral density. Thus, the density increase by ionization

during a  $1 \mu s$  time interval is  $\Delta n_e \approx 4 \times 10^9 \text{ cm}^{-3}$  or  $\Delta n_e / n_e \approx 2\%$ . With increasing time, the temperature decreases and ionization effects become negligible. These small density changes cannot be resolved with Langmuir probes whose accuracy is of order 10%. To first order, heat transport in a uniform plasma dominated by Coulomb collisions is observed. Electron-neutral collisions are negligible due to the Ramsauer effect in argon (at  $kT_e = 1$  eV,  $v_{en} \approx 7 \times 10^4 \text{ s}^{-1} \ll v_{ei} \approx 6 \times 10^6 \text{ s}^{-1} \ll \omega_{ce} = 2.6 \times 10^8 \text{ s}^{-1}$ ) [6]. The sign and magnitude of the long-lasting magnetic field are consistent with electron diamagnetism. Reversal of the external magnetic field,  $\mathbf{B}_0$ , changes the sign of  $B_z$ . The pressure balance equation,  $n \Delta kT_e + (B_0 - B_z)^2 / 2\mu_0 = B_0^2 / 2\mu_0$ , relates the temperature increase in the heated channel

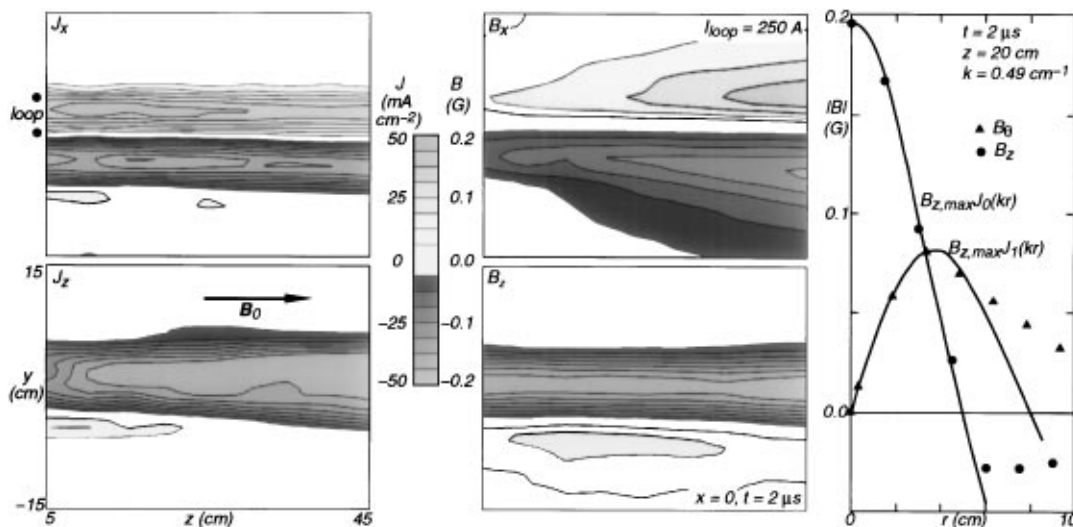


FIG. 3. Spatial distribution of perturbed magnetic field components,  $B_\theta$ ,  $B_z$ , and corresponding current densities,  $J_\theta$ ,  $J_z$ . The radial dependence of the magnetic field follows the Bessel function solutions of  $\nabla \times \mathbf{B} = k\mathbf{B}(\mathbf{r}, t)$ .

to the diamagnetic field by  $\Delta kT_e = |B_z|B_0/(\mu_0 n) \approx 3.7|B_z|$  eV/G. During the relaxation process, probe and diamagnetic measurements are consistent implying that radial electric fields are small compared to  $\nabla kT_e/e$ .

Figure 3 displays the diamagnetic field,  $B_z$ , and current,  $J_\theta = -n\nabla kT_e \times \mathbf{B}_0/B_0^2$ , at a fixed time,  $t = 2 \mu\text{s}$ , in the  $y$ - $z$  plane on the axis of the antenna. Furthermore, a comparably strong axial current,  $J_z$ , and corresponding field,  $B_\theta$ , are observed.  $J_z$  is driven by axial temperature gradients. Alternatively, it may be explained by the twisting of frozen-in magnetic field lines due to the differential electron diamagnetic drift, which is largest at the high temperature end and zero at the cold end of the flux tube. This process is the electron MHD analog to the twisting of solar MHD flux ropes by foot-point motion [7]. The magnetic helicity generated is negative (left-handed twist) when  $B_0 > 0$  and positive for  $B_0 < 0$ , since only  $J_\theta$ , but not  $J_z$ , reverses sign with  $\mathbf{B}_0$ . In the heated flux tube, the perturbed field closely matches the relation  $\nabla \times \mathbf{B} = k\mathbf{B}$ . In cylindrical geometry, with  $\partial/\partial\theta \approx \partial/\partial z \approx 0$ , the theoretical profiles are given by Bessel functions,  $B_z \propto J_0(kr)$ ,  $B_\theta \propto J_1(kr)$ . Figure 3 shows a comparison of the observed and theoretical radial profiles which have been matched at  $J_0(2.4) = 0$  to yield  $k \approx 0.49 \text{ cm}^{-1}$ . The magnetic field is twisted by an angle  $\theta \approx B_\theta/(B_0 - B_z)(L_\parallel)/r$ , where  $L_\parallel \approx 250 \text{ cm}$  is the axial length of the flux tube and  $r \approx 5 \text{ cm}$  is the radius at  $B_{\theta,\text{max}} \approx 0.1 \text{ G}$ . Although  $\theta$  is rather small (0.3 rad) for the present parameters ( $kT_e = 1 \text{ eV}$ ),  $\theta$  increases rapidly with  $kT_e$ , since  $B_\theta \propto J_\theta r \propto \sigma_\parallel \nabla_\parallel T_e r \propto T_e^{5/2} r/L_\parallel$ . With  $\theta = 0.3(kT_e/1 \text{ eV})^{5/2}[1 - (0.04kT_e/1 \text{ eV})]^{-1/2}$  rad, one finds already at  $kT_e = 5 \text{ eV}$  that  $\theta \approx 6\pi$  rad, as sketched in Fig. 1. Even larger twists may arise in solar plasmas.

Since  $\nabla \cdot \mathbf{J} \approx 0$ , the observed axial variation of  $J_z$  implies a radial current,  $J_r$ , which is two orders of magnitude smaller than  $J_z$ . The current closure within the plasma is shown below for a shorter, heated channel. These currents have important consequences on the heat transport. The axial current corresponds to a drift of hot electrons along  $\mathbf{B}_0$  away from the heat source, and the radial currents convect heat across  $\mathbf{B}_0$  out of the flux tube. The diamagnetic current creates a circulating heat flow such that  $\partial T_e/\partial\theta \approx 0$ .

The temperature decay is obtained from the diamagnetic field,  $B_z$ , whose space-time dependence is shown in Fig. 4,  $B_z(r = 0, z, t) = 0.27|\Delta kT_e|$  G/eV. The typical decay time on axis at  $z = 20 \text{ cm}$  is  $\tau_T = -B_z/(\partial B_z/\partial t) \approx 14 \mu\text{s}$  (bottom trace). This decay time can be compared with the theoretical value due to radial heat conduction, governed by the transport equation  $\frac{3}{2}d(nkT_e)/dt = -\nabla_\perp \cdot \mathbf{q}$ , where  $\mathbf{q} = -\kappa_\perp \nabla_\perp kT_e$  is the gradient heat flux,  $\kappa_\perp = 4.7nkT_e/(m\omega_{ce}^2\tau_{ei})$  is the thermal cross-field conductivity, and  $\tau_{ei} = 3.4 \times 10^5 kT_e^{3/2}/n\lambda$  is the electron collision time [8]. With  $nkT_e = nkT_{e0} + |B_z|B_0/\mu_0$ , where  $kT_{e0} \approx 0.5 \text{ eV}$  is the ambient temperature, and  $|B_z|B_0/\mu_0$  the energy increase in the flux tube, the

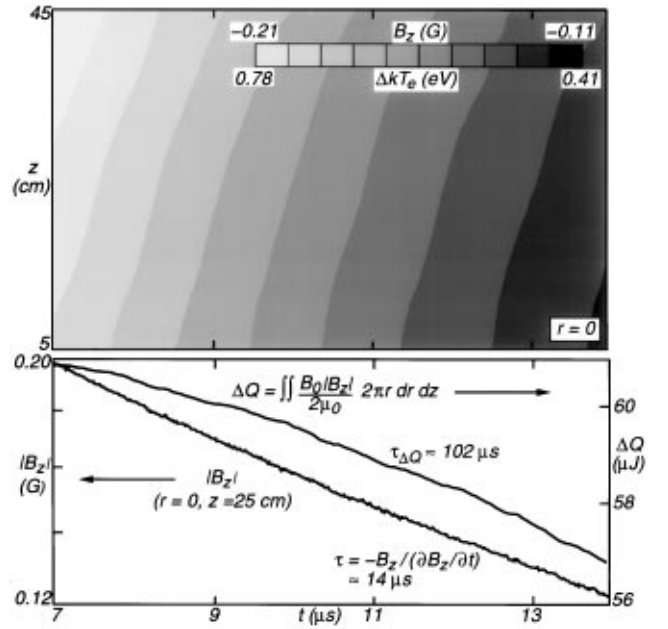


FIG. 4. Diamagnetic field  $B_z(z, t)$  indicating the electron temperature decay on axis ( $r = 0$ ). Single trace of  $B_z(z = 30 \text{ cm}, t)$  shows a decay time,  $\tau \approx 14 \mu\text{s}$ , dominated by radial heat losses. The volume-integrated energy density,  $Nk\Delta T_e(t) = B_0/\mu_0 \iint |B_z| 2\pi r dr dz$ , decays with  $\tau_\parallel \approx 102 \mu\text{s}$ , consistent with convective heat losses along  $\mathbf{B}_0$ .

transport equation can be written as  $\partial|B_z|/\partial t = 6.5 \times 10^5 \text{ cm}^2/\text{s} (1/r) \partial[(\partial|B_z|)/\partial r]/\sqrt{(1 + |B_z|/0.04 \text{ G})}/\partial r$ . From the measured dependence of  $B_z(r)$ , a radially averaged decay time of  $\tau_T = -B_z/(\partial B_z/\partial t) \approx 7.5 \mu\text{s}$  has been evaluated which predicts the observed value to within a factor of less than 2.

In order to consider the axial heat losses, the diamagnetic field is radially and axially integrated which yields the total heat deposited in the measurement volume,  $Q(t) = N\Delta kT_e = (2\pi B_0/\mu_0) \iint |B_z| r dr dz$  (Fig. 4, bottom trace). Its decay time,  $\tau_\parallel \approx 102 \mu\text{s}$ , is an order of magnitude slower than that of the temperature in the flux tube, implying that the cross-field heat losses exceed the parallel heat losses. Theoretically, the axial heat transport is given by  $\frac{3}{2}d(nkT_e)/dt = -\nabla_\parallel \cdot \mathbf{q}$ , where the heat flux,  $\mathbf{q} = 0.71nkT_e \mathbf{v}_\parallel$ , is dominated by the axial current,  $J_z = -nev_\parallel$ , rather than temperature gradients. The temporal decay of the total excess heat in the measurement volume is given by the net outflow of heat through the end surfaces,  $\frac{3}{2}dQ/dt = -\oint \mathbf{q} \cdot d\mathbf{S} \approx 2\pi \int q_\parallel r dr \approx 0.71(B_0/ne\mu_0) \int B_z J_z 2\pi r dr$ , which yields a decay time,  $\tau_\parallel = -Q/(dQ/dt) \approx 63 \mu\text{J}/0.58 \text{ W} \approx 109 \mu\text{s}$ , in good agreement with the observed value.

Knowing the total heat deposited in the column,  $Q \approx 230 \mu\text{J}$  for  $5 < z < 150 \text{ cm}$ ,  $t = 2 \mu\text{s}$ , we can make a comparison with the energy injected by the whistler wave pulse,  $U_{em} = \oint (\mathbf{E} \times \mathbf{H}) \cdot d\mathbf{S} dt$ . Here the axial component of the Poynting vector,  $E_r B_\theta/\mu_0 \approx (B_0/ne\mu_0) J_\theta B_\theta$  has been integrated at  $z = 5 \text{ cm}$  over the transverse cross

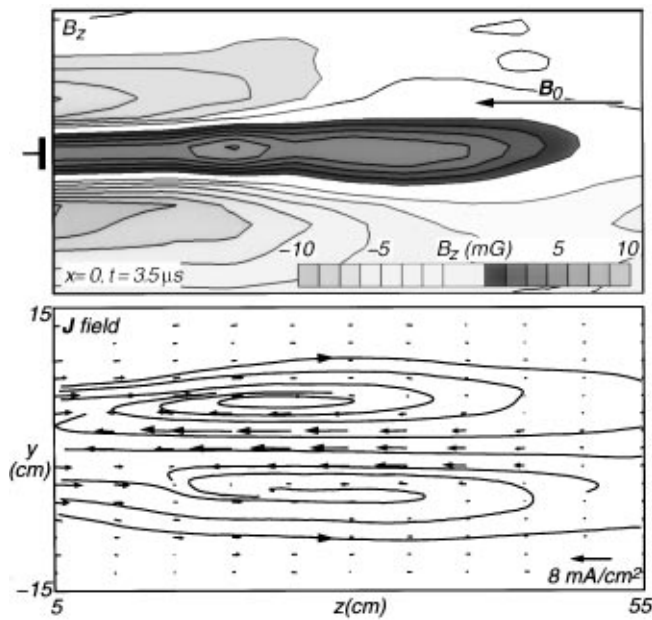


FIG. 5. Diamagnetic field,  $B_z(y, z)$ , and current density,  $(J_y, J_z)$  for a weak heating pulse applied to a disk electrode (20 A,  $\Delta t \approx 0.2 \mu\text{s}$ ). Results show the finite axial penetration depth of the heat, the current closure within the plasma, the effect of reversing  $\mathbf{B}_0$ , the independence of the method of heating, and the sensitivity of the temperature diagnostics ( $\Delta kT_{e,\text{max}} \approx 0.03 \text{ eV}$ ).

section,  $dS = 2\pi r dr$ , and the duration of the pulse,  $0 < t < 2 \mu\text{s}$ , with a result of  $U_{em} \approx 10 \mu\text{J}$ . Thus, the wave contributes only 4% of the heat while 96% comes from the near zone fields of the antenna, a result of possible interest to helicon plasma sources [9]. The real part of the antenna impedance is definitely not a radiation resistance.

The antenna current, i.e., the heat input, determines not only the temperature rise ( $\Delta kT_e = 0.003 I_{\text{loop}} \text{ eV/A}$  at  $r = 0, z = 30 \text{ cm}, t = 4.5 \mu\text{s}$ ) but also the length of the heated channel. At lower currents, the enhanced axial temperature profile ends well before the end of the device, implying that the injected heat diffuses across  $\mathbf{B}_0$  before being axially lost at the walls. The axial current loop fully closes within the plasma. As an example, Fig. 5 shows the diamagnetic field and the axial current loop of a heated flux tube during its stationary but decaying phase.  $\mathbf{B}_0$  has been reversed to show that only  $B_z$  but not  $J_z$  changes sign. Furthermore, the heating is accomplished by applying the current pulse to a disk electrode rather than a loop antenna, demonstrating that the method of heating does not affect the late relaxation processes. Both the outflow of hot electrons,  $\mathbf{v}_e = -\mathbf{J}/ne$ , from the

right end of the heated flux tube and the inflow of colder electrons at the left end cause convective heat losses resulting in a temperature peak in the middle. In Fig. 3, this peak must be at  $z \gg 45 \text{ cm}$  as judged by the weak, positive axial gradients in  $B_z$  and  $J_z$ . The axial length of the heated flux tube increases with temperature because the ratio of parallel to perpendicular heat flow increases,  $q_{u,\parallel}/q_{T,\perp} \propto kT_e J_z / \kappa_{\perp} \nabla_{\perp} T_e \propto \nu_{ei}^{-1} \propto T_e^{3/2}$ . When the heated flux tube lies within the measurement volume, the decay time of the total energy,  $Q(t) = N\Delta kT_e$ , is  $\tau_{\parallel} \gg 100 \mu\text{s}$ , the exact value being subject to significant bit noise errors. The temperature equilibration time with ions is  $\tau \approx (m_i/2m_e)\nu_{ei}^{-1} \approx 2.4 \text{ ms}$ , while the temperature decay time of the entire plasma column is observed to be  $\tau_T \approx 0.9 \text{ ms}$  for  $kT_e \approx 0.5 \text{ eV}$  [10].

In summary, sudden local electron heating generates helicity since the ‘‘foot-point’’ diamagnetic rotation twists the frozen-in magnetic field lines. The associated electron currents conserve charge ( $\nabla \cdot \mathbf{J} = 0$ ) but convect heat out of the flux tube ( $\nabla \cdot \mathbf{q} = -\mathbf{J} \cdot \nabla kT_e/e \neq 0$ ). Although beyond the resolution of present experiments, such electron MHD effects may arise as a fine structure in solar plasmas.

The authors gratefully acknowledge support for this work from NSF Grant No. PHY93-03821.

- [1] N. J. Lopes Cardozo *et al.*, in *International Conference on Plasma Physics ICPP 1994*, edited by P. H. Sakanaka and M. Tendler, AIP Conf. Proc. No. 345 (AIP Press, New York, 1995), p. 135.
- [2] E. R. Priest, in *Solar System Plasmas in Space and Time*, edited by J. L. Burch and J. H. Waite, Jr., Geophys. Monograph No. 84 (AGU, Washington, DC, 1994), p. 1.
- [3] J. M. Urrutia, R. L. Stenzel, and C. L. Rousculp, *Phys. Plasmas* **2**, 1100 (1995).
- [4] P. J. Cargill, in *Solar System Plasmas in Space and Time*, edited by J. L. Burch and J. H. Waite, Jr., Geophys. Monograph No. 84 (AGU, Washington, DC, 1994), p. 21.
- [5] J. M. Urrutia and R. L. Stenzel, *Phys. Rev. Lett.* **67**, 1867 (1991).
- [6] S. C. Brown, *Basic Data of Plasma Physics* (MIT Press, Cambridge, MA, 1966), p. 27.
- [7] E. N. Parker, in *Magnetic Reconnection in Space and Laboratory Plasmas*, edited by E. W. Hones, Geophys. Monograph No. 30 (AGU, Washington, DC, 1984), p. 33.
- [8] J. D. Huba, *NRL Plasma Formulary* (NRL, Washington, DC, 1994), p. 36.
- [9] F. F. Chen, *Plasma Phys. Controlled Fusion* **33**, 339 (1991).
- [10] R. L. Stenzel, *Phys. Fluids B* **1**, 1369 (1989).